An Improved Fourier–Ritz Method for Analyzing In-Plane Free Vibration of Sectorial Plates

Siyuan Bao[1]
School of Civil Engineering,
University of Science and Technology of Suzhou,
Suzhou 215011, China;
School of Mechanical and
Aerospace Engineering,
Oklahoma State University,
Stillwater, OK 74078
e-mail: sy.bgwl.bao@hotmail.com

Shuodao Wang
School of Mechanical and
Aerospace Engineering,
Oklahoma State University,
Stillwater, OK 74078

Bo Wang
School of Mechanical and
Aerospace Engineering,
Oklahoma State University,
Stillwater, OK 74078

A modified Fourier–Ritz approach is developed in this study to analyze the free in-plane vibration of orthotropic annular sector plates with general boundary conditions. In this approach, two auxiliary sine functions are added to the standard Fourier cosine series to obtain a robust function set. The introduction of a logarithmic radial variable simplifies the expressions of total energy and the Lagrangian function. The improved Fourier expansion based on the new variable eliminates all the potential discontinuities of the original displacement function and its derivatives in the entire domain and effectively improves the convergence of the results. The radial and circumferential displacements are formulated with the modified Fourier series expansion, and the arbitrary boundary conditions are simulated by the artificial boundary spring technique. The number of terms in the truncated Fourier series and the appropriate value of the boundary spring retraining stiffness are discussed. The developed Ritz procedure is used to obtain accurate solution with adequately smooth displacement field in the entire solution domain. Numerical examples involving plates with various boundary conditions demonstrate the robustness, precision, and versatility of this method. The method developed here is found to be computationally economic compared with the previous method that does not adopt the logarithmic radial variable. [DOI: 10.1115/1.4037030]

Keywords: sectorial plate, in-plane vibration, improved Fourier–Ritz method, logarithmic radial variable

1 Introduction

Circular and sector plates are widely used in engineering practice as components of different structures such as airplane wings, building walls, floor slabs, and loaded membrane and even in nuclear engineering. It is critically important to understand the dynamic characteristics of such structures in order to ensure reliable structural performance. Having extensively investigated the vibration of plates of various shapes, support, and loading conditions, many researchers have made great efforts on this problem using a large number of different methods [1–9]. For one case: natural vibration of thick plate, a comprehensive survey of the references up to 1994 can be found in Ref. [5]. However, majority of the previous studies focus on the out-of-plane vibration of plates [1–5] rather than in-plane vibration [6–9]. Recently, it was found that the in-plane vibration has a significant effect on the sound radiation and transmissions of vibration energies in build-up structures [10], and determination of natural in-plane vibrating frequencies of plates within the medium to high-frequency range is also important and has always been a challenging problem. Therefore, a better understanding on the in-plane vibration behaviors of plates is required to design these structures properly.

The use of Levy-type (or single series) solutions in vibration analysis of elastic plates or shells has been remained as one of the most economic approaches in structural mechanics. The most attractive feature of this strategy lies in its ability to apply in different problems with a range of boundary conditions and variable mechanical properties (for plates with variable thickness, functionally graded materials, laminated structures, etc.). In solving the in-plane problem, it is an important factor to represent or approximate the displacement field properly. Let us briefly review relevant works of free-in-plane vibration of the orthotropic circular and sector plates. Onoe [6] used special functions to express the circumferential and radial displacements on basis of the Love's theory. Holland [7] and Farag and Pan [11] applied trigonometric and Bessel functions in representing the mode shape. Chen and Liu [12] investigated the thin plates of different shapes and used a least-square method to satisfy the boundary conditions. For circular and annular plates, Irie et al. [8] utilized the transfer matrix method. For circular annular plates with periodicity in the circumferential direction, Bashmal et al. [13] presented a generalized Rayleigh–Ritz method. Park [14] derived the frequency equations corresponding to the in-plane vibration using Hamilton's principle. For the free in-plane vibrations of an annular sector plate, Seok and Tiersten [15] solved the problem by a variational approximation procedure. Ravari and Forouzan [16] did relevant vibrating plane problems for circular annular plates by using stress–strain–displacement expressions. Vladimir et al. [17] adopted the displacement potentials to study the free in-plane vibration of the rectangular, annular, and circular plates. The work of Kim et al. [18] is based on a new assumption of the mode shapes relevant with the number of nodal diameters. Some numerical researches are also made. For example, Singh and Muhammad [19] presented a numerical method to study the free in-plane vibration of the isotropic nonrectangular plate by means of interpolation technology. Leung et al. [9] used a Fourier p-element in analyzing the vibrating plane problems.

It should be emphasized that Wang et al. [20] used a modified Fourier–Ritz approach to solve for the free in-plane vibration of orthotropic circular, annular, and sector plates subjected to general boundary conditions. The Fourier–Ritz approach was first proposed by Li [21,22], who combined the modified Fourier series technique and Ritz method. Recently, this modified Fourier series technique has attracted a lot of attentions and is widely used in the vibration analysis of plate and shell structures with general boundary conditions [23–29]. The authors discussed the free out-of-plane or in-plane vibrations of plates or shells in various shapes.

[1]Corresponding author.

Contributed by the Applied Mechanics Division of ASME for publication in the Journal of Applied Mechanics. Manuscript received March 10, 2017; final manuscript received June 7, 2017; published online July 7, 2017. Assoc. Editor: George Kardomateas.

To analyze the static bending problems of sector plates, Yao et al. [30] presented the symplectic method in which the logarithmic radial variable is used. Kim and Yoo [31] adopted a new type of variable to obtain an analytic solution to the flexural responses of annular sector thin plates.

In the current study, a new variable relevant to the radius, the logarithm of the radius, is introduced to investigate the in-plane free vibration of annular sector plates with classical and elastic boundary conditions. The method is based on the modified Fourier–Ritz approach and extends previous research [20] to be applicable to the free in-plane vibration of sectorial plate structures under general boundary conditions. In this method, the two in-plane displacement functions are formulated in 2D Fourier cosine series, and the auxiliary functions are two sin functions. The introduction of the auxiliary functions ensures and accelerates the convergence of the Fourier series. Then, the Ritz procedure is used to obtain the unknown expanded coefficients and solve the eigenvalue and eigenvector problems.

Our main work focuses on presenting the basic simplified theory with the use of the logarithmic radial variable, then the global stiffness matrix and mass matrix can be expressed in a much simpler explicit form, and the integration can also be performed explicitly. These advantages significantly reduce the computation cost compared to the previous theories that do not use the logarithmic radial variable. Moreover, for a given solution accuracy, the number of terms in the truncated Fourier series is less than that in the previous method [20]. Compared to Ref. [20], the stiffness matrix is simplified significantly as the element of the stiffness matrix is explicit, which need not be the tedious process of numerical integration. What's more, the dimension of the matrix in the eigenproblem is also smaller as fewer terms in the truncated series are needed. Comparison of computation and convergence rate shows the significance of the method.

2 The Basic Theory

2.1 Preliminaries. The analysis starts with an orthotropic annular sector plate with uniform thickness h, inner radius R_0, outer radius R_1, and sector angle ϕ, as shown in Fig. 1. Displacements of the plate in the r- and θ-directions are denoted by $u = u(r, \theta, t)$ and $v = v(r, \theta, t)$, respectively, where t denotes time.

General support conditions are considered, which are realized by massless normal and tangential springs along each edge. Out-of-plane bending is not considered in this study, and constraints against out-of-plane rotation are not imposed. Similar to the discussion by Dozio [32], the stiffness values of each restraining spring at different locations and directions are introduced. The symbol k_γ^δ stands for the spring restraining stiffness, with its subscripts $\gamma = R_0, \theta_0, R_1$, and θ_1 referring to the inner, bottom, outer, and upper edges, respectively, and $\delta = U, V$ denoting the normal and tangential directions, respectively. For instance, $k_{\theta 0}^U$ indicates the stiffness values for springs in the surface normal direction along the bottom edge of the plate. The stiffness for each of the elastic restraints can vary as a function along an edge, i.e., $k_\gamma^\delta = k_\gamma^\delta(\theta)$ for $\gamma = R_0, R_1$ and $k_\gamma^\delta = k_\gamma^\delta(r)$ for $\gamma = \theta_0, \theta_1$.

A set of appropriate stiffness values can be selected to simulate classical boundary conditions, such as clamped, free, simply supported, and elastically supported conditions that can be cataloged into two kinds as discussed by Gorman [33] in the case of in-plane vibration. Table 1 in Sec. 3 summarizes the stiffness values that correspond to various boundary conditions.

For general supported orthotropic sector plates, based on the force equilibrium at the four edges, the boundary conditions corresponding to the elastic spring can be expressed as

$$k_{Ri}^U u = A_{rr}\frac{\partial u}{\partial r} + A_{r\theta}\frac{1}{r}\left(u + \frac{\partial v}{\partial \theta}\right),$$
$$k_{Ri}^V v = G_{r\theta}\left(\frac{1}{r}\frac{\partial u}{\partial \theta} + \frac{\partial v}{\partial r} - \frac{v}{r}\right) \quad (i = 0, 1) \tag{1}$$

$$k_{\theta i}^V u = A_{\theta r}\frac{\partial u}{\partial r} + A_{\theta\theta}\frac{1}{r}\left(u + \frac{\partial v}{\partial \theta}\right),$$
$$k_{\theta i}^U v = -G_{r\theta}\left(\frac{1}{r}\frac{\partial u}{\partial \theta} + \frac{\partial v}{\partial r} - \frac{v}{r}\right) \quad (i = 0, 1) \tag{2}$$

where $A_{rr} = (E_r/(1 - \mu_r\mu_\theta)), A_{\theta\theta} = (E_\theta/(1 - \mu_r\mu_\theta))$, and $A_{r\theta} = (\mu_r E_\theta/(1 - \mu_r\mu_\theta))$ are the in-plane tensile stiffnesses, $G_{r\theta}$ is the shear Young's modulus, and E_z and μ_z ($z = r$ or θ) are Young's modulus and Poisson's ration in the z directions, respectively.

The strain energy V_{pl} of the sector plate is obtained as

$$V_{pl} = \frac{h}{2}\int_{R_0}^{R_1}\int_0^\phi \left[A_{rr}\left(\frac{\partial u}{\partial r}\right)^2 + A_{\theta\theta}\frac{1}{r^2}\left(u + \frac{\partial v}{\partial \theta}\right)^2 + 2A_{r\theta}\frac{1}{r}\frac{\partial u}{\partial r}\left(\frac{\partial v}{\partial \theta} + u\right) + G_{r\theta}\left(\frac{1}{r}\frac{\partial u}{\partial \theta} + \frac{\partial v}{\partial r} - \frac{v}{r}\right)^2\right] r\,dr\,d\theta \tag{3}$$

Normal and tangential boundary restraining springs are arranged around all the plate edges to simulate the boundary conditions. The potential energy V_s stored in the boundary springs is written as

$$V_s = \frac{1}{2}\int_0^\phi \left[R_0\left(k_{R0}^U u^2 + k_{R0}^V v^2\right)\Big|_{r=R_0} + R_1\left(k_{R1}^U u^2 + k_{R1}^V v^2\right)\Big|_{r=R_1}\right] d\theta + \frac{1}{2}\int_{R_0}^{R_1}\left[\left(k_{\theta 0}^U u^2 + k_{\theta 0}^V v^2\right)\Big|_{\theta=0} + \left(k_{\theta 1}^U u^2 + k_{\theta 1}^V v^2\right)\Big|_{\theta=\phi}\right] r\,dr \tag{4}$$

Adding the strain energy V_{pl} and the potential energy V_s together yields

$$V = \frac{h}{2}\int_{R_0}^{R_1}\int_0^\phi \left[A_{rr}\left(\frac{\partial u}{\partial r}\right)^2 + A_{\theta\theta}\frac{1}{r^2}\left(u + \frac{\partial v}{\partial \theta}\right)^2 + 2A_{r\theta}\frac{1}{r}\frac{\partial u}{\partial r}\left(\frac{\partial v}{\partial \theta} + u\right) + G_{r\theta}\left(\frac{1}{r}\frac{\partial u}{\partial \theta} + \frac{\partial v}{\partial r} - \frac{v}{r}\right)^2\right] r\,dr\,d\theta + \frac{1}{2}\int_0^\phi \left[R_0\left(k_{R0}^U u^2 + k_{R0}^V v^2\right)\Big|_{r=R_0} + R_1\left(k_{R1}^U u^2 + k_{R1}^V v^2\right)\Big|_{r=R_1}\right] d\theta + \frac{1}{2}\int_{R_0}^{R_1}\left[\left(k_{\theta 0}^U u^2 + k_{\theta 0}^V v^2\right)\Big|_{\theta=0} + \left(k_{\theta 1}^U u^2 + k_{\theta 1}^V v^2\right)\Big|_{\theta=\phi}\right] dr \tag{5}$$

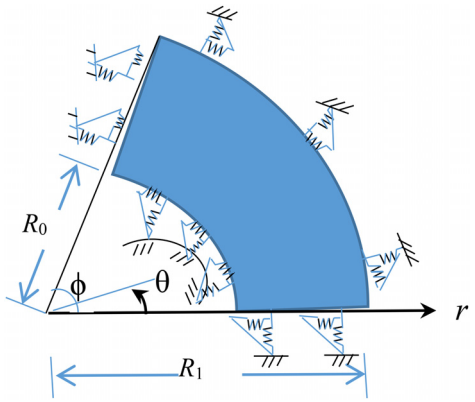

Fig. 1 An orthotropic annular sector plate with arbitrary in-plane elastic edge supports

The kinetic energy T of the sector plate is

$$T = \frac{\bar{\rho}h}{2}\int_{R_0}^{R_1}\int_0^{\phi}\left[\left(\frac{\partial u}{\partial t}\right)^2 + \left(\frac{\partial v}{\partial t}\right)^2\right] r\mathrm{d}r\mathrm{d}\theta \tag{6}$$

where $\bar{\rho}$ is the plate's mass density. Considering an harmonic motion with frequency ω, i.e.,

$$\begin{cases} u(r,\theta,t) = \bar{u}(r,\theta)e^{j\omega t} = \bar{u}e^{j\omega t} \\ v(r,\theta,t) = \bar{v}(r,\theta)e^{j\omega t} = \bar{v}e^{j\omega t} \end{cases} \tag{7}$$

the maximum strain energy $V_{\max}$ and the maximum kinetic energy $T_{\max}$ for the plate are

$$\begin{aligned} V_{\max} = &\frac{h}{2}\int_{R_0}^{R_1}\int_0^{\phi}\left[A_{rr}\left(\frac{\partial \bar{u}}{\partial r}\right)^2 + A_{\theta\theta}\frac{1}{r^2}\left(\bar{u}+\frac{\partial \bar{v}}{\partial \theta}\right)^2\right. \\ &\left. +2A_{r\theta}\frac{1}{r}\frac{\partial \bar{u}}{\partial r}\left(\frac{\partial \bar{v}}{\partial \theta}+\bar{u}\right) + G_{r\theta}\left(\frac{1}{r}\frac{\partial \bar{u}}{\partial \theta}+\frac{\partial \bar{v}}{\partial r}-\frac{\bar{v}}{r}\right)^2\right] r\mathrm{d}r\mathrm{d}\theta \\ &+\frac{1}{2}\int_0^{\phi}\left[R_0\left(k_{R0}^U\bar{u}^2+k_{R0}^V\bar{v}^2\right)\Big|_{r=R_0} + R_1\left(k_{R1}^U\bar{u}^2+k_{R1}^V\bar{v}^2\right)\Big|_{r=R_1}\right]\mathrm{d}\theta \\ &+\frac{1}{2}\int_{R_0}^{R_1}\left[\left(k_{\theta0}^U\bar{u}^2+k_{\theta0}^V\bar{v}^2\right)\Big|_{\theta=0} + \left(k_{\theta1}^U u^2+k_{\theta1}^V\bar{v}^2\right)\Big|_{\theta=\phi}\right]\mathrm{d}r \end{aligned} \tag{8}$$

and

$$T_{\max} = \frac{\bar{\rho}h\omega^2}{2}\int_{R_0}^{R_1}\int_0^{\phi}(\bar{u}^2+\bar{v}^2) r\mathrm{d}r\mathrm{d}\theta \tag{9}$$

respectively. According to the conventional Ritz approximation, the following solutions are assumed for the displacements amplitudes $\bar{u}$ and $\bar{v}$:

$$\begin{cases} \bar{u} = \sum_{m=1}^{M}\sum_{n=1}^{N} a_{mn}\chi_m(r)\zeta_n(\theta) \\ \bar{v} = \sum_{m=1}^{M}\sum_{n=1}^{N} b_{mn}\chi_m(r)\zeta_n(\theta) \end{cases} \tag{10}$$

where a_{mn} and b_{mn} are the unknown coefficients, and $\chi_m(r)$ and $\zeta_n(\theta)$ are the appropriate admissible functions. As pointed out by Budiansky and Hu [34], the geometrical boundary conditions of the problem need to be satisfied by the summation of the whole set of admissible functions, but do not have to be satisfied by each term in the expansion.

2.2 The Logarithmic Radial Variable and the Improved Theory. In this study, a new variable ρ is introduced as $r = e^{\rho}$, then as pointed out in Ref. [31], taking logarithm and differentiating both terms of the relationship yield

$$\frac{\mathrm{d}\rho}{\mathrm{d}r} = \frac{\mathrm{d}(\ln r)}{\mathrm{d}r} = \frac{1}{r} \tag{11}$$

Using Eq. (11), the following is obtained:

$$\frac{\partial Q(r,\theta)}{\partial r} = \frac{1}{r}\frac{\partial Q_1(\rho,\theta)}{\partial \rho} \tag{12}$$

where $Q(r,\theta)$ stands for an arbitrary function varying with r and θ, and $Q_1(\rho,\theta)$ is $Q(r,\theta)$ written with the variable ρ. Substituting Eq. (12) into Eqs. (8) and (9), we have

$$\begin{aligned} V_{\max} = &\frac{h}{2}\int_{\ln R_0}^{\ln R_1}\int_0^{\phi}\left[A_{rr}\left(\frac{\partial u}{\partial \rho}\right)^2 + A_{\theta\theta}\left(u+\frac{\partial v}{\partial \theta}\right)^2\right. \\ &\left. +2A_{r\theta}\frac{\partial u}{\partial \rho}\left(\frac{\partial v}{\partial \theta}+u\right) + G_{r\theta}\left(\frac{\partial u}{\partial \theta}+\frac{\partial v}{\partial \rho}-v\right)^2\right]\mathrm{d}\rho\mathrm{d}\theta \\ &+\frac{1}{2}\int_0^{\phi}\left[R_0\left(k_{R0}^U u^2+k_{R0}^V v^2\right)\Big|_{\rho=\ln R_0}\right. \\ &\left. +R_1\left(k_{R1}^U u^2+k_{R1}^V v^2\right)\Big|_{\rho=\ln R_1}\right]\mathrm{d}\theta \\ &+\frac{1}{2}\int_{\ln R_0}^{\ln R_1}\left[\left(k_{\theta0}^U u^2+k_{\theta0}^V v^2\right)\Big|_{\theta=0} + \left(k_{\theta1}^U u^2+k_{\theta1}^V v^2\right)\Big|_{\theta=\phi}\right]e^{\rho}\mathrm{d}\rho \end{aligned} \tag{13}$$

and

$$T_{\max} = \frac{\bar{\rho}h\omega^2}{2}\int_{\ln R_0}^{\ln R_1}\int_0^{\phi}(u^2+v^2)e^{2\rho}\mathrm{d}\rho\mathrm{d}\theta \tag{14}$$

In using the Ritz method, the energy functional is defined by Lagrangian function as

$$L = V - T \tag{15}$$

To further simplify the expressions, a new variable $\xi = \rho - \ln R_0 = \ln(r/R_0)$ is introduced. Equations (13) and (14) become

$$\begin{aligned} V_{\max} = &\frac{h}{2}\int_0^{L_R}\int_0^{\phi}\left[A_{rr}\left(\frac{\partial u}{\partial \xi}\right)^2 + A_{\theta\theta}\left(u+\frac{\partial v}{\partial \theta}\right)^2\right. \\ &\left. +2A_{r\theta}\frac{\partial u}{\partial \xi}\left(\frac{\partial v}{\partial \theta}+u\right) + G_{r\theta}\left(\frac{\partial u}{\partial \theta}+\frac{\partial v}{\partial \xi}-v\right)^2\right]\mathrm{d}\xi\mathrm{d}\theta \\ &+\frac{1}{2}\int_0^{\phi}\left[R_0\left(k_{R0}^U u^2+k_{R0}^V v^2\right)\Big|_{\xi=0} + R_1\left(k_{R1}^U u^2+k_{R1}^V v^2\right)\Big|_{\xi=L_R}\right]\mathrm{d}\theta \\ &+\frac{1}{2}R_0\int_0^{L_R}\left[\left(k_{\theta0}^U u^2+k_{\theta0}^V v^2\right)\Big|_{\theta=0} + \left(k_{\theta1}^U u^2+k_{\theta1}^V v^2\right)\Big|_{\theta=\phi}\right]e^{\xi}\mathrm{d}\xi \end{aligned} \tag{16}$$

Table 1 Convergence of frequency parameters Ω for the circular sectorial plate with different spring stiffnesses

		Value of spring stiffness						Value of spring stiffness		
Mode	R_0/R_1	10^5	10^6	10^7	10^8	FE results	R_0/R_1	10^5	10^6	10^7
1	1/20	2.8772	2.8810	2.8711	3.2853	2.8737[a]	1/40	2.8818	2.8808	3.1621
2	1/20	4.3531	4.3527	4.3438	4.0873	4.3478[a]	1/40	4.3548	4.3558	4.3783
3	1/20	4.3807	4.3757	4.3963	4.2211	4.3632[a]	1/40	4.3832	4.3769	4.4701
4	1/20	5.7992	5.8113	5.8366	5.8871	5.7913[a]	1/40	5.8189	5.8332	5.7949

[a]Results from Ref. [20].

and

$$T_{\max} = \frac{\bar{\rho} h \omega^2}{2} R_0^2 \int_0^{L_R} \int_0^{\phi} (u^2 + v^2) e^{2\xi} \mathrm{d}\xi \mathrm{d}\theta \tag{17}$$

respectively, where $L_R = \ln(R_1/R_0)$.

All the items in Eq. (16) have constant coefficients for the strain energy terms, while in Eq. (8) most of the corresponding coefficients vary with respect to the radius r. Moreover, the starting values of the definite integration in the ξ, θ directions are all from zero, which is more convenient for further derivations.

With the new variable ξ, boundary conditions corresponding to Eqs. (1) and (2) become

$$\begin{aligned} k_{Ri}^U e^{\xi} u &= A_{rr} \frac{\partial u}{\partial \xi} + A_{r\theta} \left(u + \frac{\partial v}{\partial \theta} \right), \\ k_{Ri}^V e^{\xi} v &= G_{r\theta} \left(\frac{\partial u}{\partial \theta} + \frac{\partial v}{\partial \xi} - v \right) \quad (i = 0, 1) \end{aligned} \tag{18}$$

$$\begin{aligned} k_{\theta i}^U e^{\xi} u &= A_{\theta r} \frac{\partial u}{\partial \xi} + A_{\theta\theta} \left(u + \frac{\partial v}{\partial \theta} \right), \\ k_{\theta i}^V e^{\xi} v &= -G_{r\theta} \left(\frac{\partial u}{\partial \theta} + \frac{\partial v}{\partial \xi} - v \right) \quad (i = 0, 1) \end{aligned} \tag{19}$$

2.3 Solution Procedure by Using the Logarithmic Radial Variable. As discussed by Wang et al. [20], the importance of choosing the admissible function is the "core work" and "the first work," which can be traced to previous studies [21,22]. Using the logarithmic radial variable, the displacements in the two directions become

$$\begin{cases} u(\xi, \theta) = \sum_{m=1}^{M} \sum_{n=1}^{N} c_{mn} f_m(\xi) g_n(\theta) \\ v(\xi, \theta) = \sum_{m=1}^{M} \sum_{n=1}^{N} d_{mn} f_m(\xi) g_n(\theta) \end{cases} \tag{20}$$

where c_{mn} and d_{mn} are the unknown coefficients, and $f_m(\xi)$ and $g_n(\theta)$ are the appropriate admissible functions. Apparently, the displacement functions in Eq. (20) are different from the original Eq. (10). The truncated expansion is adopted for the convenience of numerical computation, and the solution can be of arbitrary precision depending on the number of the terms included. In actual calculations, the value of M and N will be selected to obtain results with acceptable accuracy.

As for the admissible functions, Ilanko et al. [35,36] presented a discussion on the characteristics of the set of admissible functions used in the Rayleigh Ritz method. The discussion includes the use of polynomials, trigonometric functions, and a combination of both.

Dozio [32] also used a trigonometric form in free in-plane vibration analysis of rectangular plates with arbitrary elastic boundary conditions. Another method to formulate the admissible functions is to use an improved Fourier expansion that considers the continuity of the derivatives of a certain order [20]. Similarly, a set of simple trigonometric series for constructing the displacement functions in this study are selected as

$$f_m(\xi) = \begin{cases} \sin\left(\xi \dfrac{m\pi}{L_R} \right), & m = 1, 2 \\ \cos\left(\xi \dfrac{(m-3)\pi}{L_R} \right), & m \geq 3 \end{cases} \tag{21}$$

$$g_n(\theta) = \begin{cases} \sin\left(\theta \dfrac{n\pi}{\phi} \right), & n = 1, 2 \\ \cos\left(\theta \dfrac{(n-3)\pi}{\phi} \right), & n \geq 3 \end{cases} \tag{22}$$

The Fourier series expansion in Eqs. (21) and (22) contains a complete series and therefore exhibits good numerical stability. Conventional Fourier series generally have the boundary convergence problems except for a few simple boundary cases. As discussed in the work of Wang et al. [20], the displacement functions should satisfy the continuity conditions and the boundary constraints, so the auxiliary functions must be closed in form and sufficiently smooth over the entire domain [0, L]. In other words, the introduction of the auxiliary function here eliminates the potential discontinuities of the displacement function and its derivatives in the whole domain. It is also significant that the auxiliary function can improve the convergent properties of Fourier series. Mathematically, the series in the form of Eqs. (20)–(22) is able to expand and uniformly converge to any function $H(\xi, \theta) \in C^1$, i.e., have up to the second derivatives for $\forall (\xi, \theta) \in D : ([0, L_R] \otimes [0, \phi])$.

Substitution of Eqs. (20)–(22) into Eqs. (16) and (17) and minimizing the function $L = U_{\max} - T_{\max}$ by performing the Ritz procedure with respect to the unknown coefficients c_{mn} and d_{mn} yield the following eigenvalue equations:

$$\begin{cases} \sum_{r=1}^{M} \sum_{s=1}^{N} [K_{mnrs}^{uu} c_{rs} + K_{mnrs}^{uv} d_{rs} - \omega^2 M_{mnrs} c_{rs}] = 0 \\ \sum_{r=1}^{M} \sum_{s=1}^{N} [K_{mnrs}^{vu} c_{rs} + K_{mnrs}^{vv} d_{rs} - \omega^2 M_{mnrs} d_{rs}] = 0 \end{cases} \tag{23}$$

The elements of the plate's global stiffness and mass matrices in Eq. (23) are given by

$$\begin{cases} K_{mnrs}^{uu} = A_{rr} I_{mr}^{11} I_{ns}^{00} + G_{r\theta} I_{mr}^{00} I_{ns}^{11} + A_{\theta\theta} I_{mr}^{00} I_{ns}^{00} + A_{r\theta} I_{ns}^{00} (I_{mr}^{10} + I_{mr}^{01}) \\ \qquad + R_0 (E_{mr}^0 J_{ns}^{r0U} + E_{mr}^1 J_{ns}^{r1U}) + (R_0 J_{mr}^{t0U} E_{ns}^0 + R_1 J_{mr}^{t1U} E_{ns}^1) \\ K_{mnrs}^{uv} = A_{\theta\theta} I_{mr}^{00} I_{ns}^{01} + A_{r\theta} I_{mr}^{10} I_{ns}^{01} + G_{r\theta} (I_{mr}^{01} - I_{mr}^{00}) I_{ns}^{10} \\ K_{mnrs}^{vv} = A_{\theta\theta} I_{mr}^{00} I_{ns}^{11} + G_{r\theta} (I_{mr}^{00} - I_{mr}^{10} - I_{mr}^{01} + I_{mr}^{11}) I_{ns}^{00} \\ \qquad + R_0 (E_{mr}^0 J_{ns}^{r0V} + E_{mr}^1 J_{ns}^{r1V}) + (R_0 J_{mr}^{t0V} E_{ns}^0 + R_1 J_{mr}^{t1V} E_{ns}^1) \end{cases} \tag{24}$$

and

$$\begin{cases} M_{mnrs}^{uu} = \bar{\rho} h R_0^2 P_{mr} I_{ns}^{00} \\ M_{mnrs}^{vv} = M_{mnrs}^{uu} \end{cases} \tag{25}$$

in which

$$\begin{cases} E_{mr}^0 = f_m(0) f_r(0), E_{ns}^0 = g_n(0) g_s(0) \\ E_{mr}^1 = f_m(L_R) f_r(L_R), E_{ns}^1 = g_n(\phi) g_s(\phi) \end{cases} \tag{26}$$

$$\begin{cases} I_{mr}^{\alpha\beta} = \int_0^{L_R} \dfrac{d^\alpha f_m}{d\xi^\alpha} \dfrac{d^\beta f_r}{d\xi^\beta} \mathrm{d}\xi, I_{ns}^{\alpha\beta} = \int_0^{\phi} \dfrac{d^\alpha g_n}{d\theta^\alpha} \dfrac{d^\beta g_s}{d\theta^\beta} \mathrm{d}\theta \\ J_{mr}^{\gamma\delta} = \int_0^{L_R} k_\gamma^\delta f_m(\xi) f_r(\xi) \mathrm{e}^{\xi} \mathrm{d}\xi, J_{ns}^{\gamma\delta} = \int_0^{\phi} k_\gamma^\delta g_n(\theta) g_s(\theta) \mathrm{d}\theta \end{cases} \tag{27}$$

$$P_{mr} = \int_0^{L_R} f_m f_r \mathrm{e}^{2\xi} \mathrm{d}\xi \tag{28}$$

When the spring stiffness of the elastic boundary is uniform, it can be found that

Table 2 The properties of materials used in the computations

	E_r/E_θ	E_θ (GPa)	μ_r	$\bar{\rho}$ (kg/m^3)	Corresponding cases
Material A	40	70	0.3	7850	Tables 1 and 4 and Fig. 2
Material B	20	70	0.3	7850	Tables 5, 7, and 8 and Fig. 3
Material C	1	206	0.3	7850	Table 6

$$J_{mr}^{\gamma\delta} = k_\gamma^\delta I_{ns}^{00} \tag{29}$$

Equation (23) can also be written in the matrix form

$$\left\{ \begin{bmatrix} \boldsymbol{K}^{uu} & \boldsymbol{K}^{uv} \\ \boldsymbol{K}^{vu} & \boldsymbol{K}^{vv} \end{bmatrix} - \omega^2 \begin{bmatrix} \boldsymbol{M}^{uu} & \boldsymbol{0} \\ \boldsymbol{0} & \boldsymbol{M}^{vv} \end{bmatrix} \right\} \begin{Bmatrix} \boldsymbol{C}^u \\ \boldsymbol{D}^v \end{Bmatrix} = \boldsymbol{0} \tag{30}$$

where

$$\begin{aligned} \boldsymbol{C}^u &= \{c_{11}, c_{12}, c_{13}, \ldots, c_{1N}, c_{21}, \ldots, c_{rs}, \ldots, c_{MN}\} \\ \boldsymbol{D}^v &= \{d_{11}, d_{12}, d_{13}, \ldots, d_{1N}, d_{21}, \ldots, d_{rs}, \ldots, d_{MN}\} \end{aligned} \tag{31}$$

By solving the eigenvalue problem in Eq. (30), the frequencies of orthotropic annular sector plates can be obtained. Substituting the obtained eigenvectors into Eq. (20) yields the corresponding mode shapes.

In this method, the integrals involved in the calculation of the mass and stiffness matrices can be obtained analytically, thus avoiding tedious numerical iterations [13] or integration [20] needed by previous methods. For the case of uniform spring stiffness k_γ^δ, with the selected admissible functions in Eqs. (21) and (22), the explicit forms of all the sub matrices, such as $\boldsymbol{K}^{uu}$, $\boldsymbol{K}^{vv}$, $\boldsymbol{K}^{uv}$, $\boldsymbol{M}^{uu}$, and $\boldsymbol{M}^{vv}$, can be obtained with the aid of several basic integration formulas in the Appendix. Moreover, these matrices can also be organized into four-block matrices as

$$\boldsymbol{Z} = \begin{bmatrix} \boldsymbol{Z}_{11} & \boldsymbol{Z}_{12} \\ \boldsymbol{Z}_{21} & \boldsymbol{Z}_{22} \end{bmatrix} \tag{32}$$

where $\boldsymbol{Z}$ can stand for $\boldsymbol{K}^{uu}$, $\boldsymbol{K}^{vv}$, $\boldsymbol{K}^{uv}$, $\boldsymbol{M}^{uu}$, and $\boldsymbol{M}^{vv}$, and $\boldsymbol{Z}_{11}, \boldsymbol{Z}_{12}, \boldsymbol{Z}_{21}, \boldsymbol{Z}_{22}$ are 2×2, $2 \times (MN-2)$, $(MN-2) \times 2$, $(MN-2) \times (MN-2)$ matrices, respectively. When the chosen admissible functions in Eqs. (21) and (22) do not include the first two terms, this corresponds to the case of conventional Fourier expansion for the in-plane displacements, and the corresponding matrix $\boldsymbol{Z}$ will degenerate to $\boldsymbol{Z}_{22}$.

Table 3 Different nondimensional spring stiffness values for general boundary conditions

	At $r =$ constant			At $\theta =$ constant		
		Stiffness values			Stiffness values	
Boundary condition	Essential conditions	Γ_U	Γ_U	Essential conditions	Γ_V	Γ_V
Free (F)	$\sigma_r = 0, \tau_{r\theta} = 0$	0	0	$\sigma_\theta = 0, \tau_{r\theta} = 0$	0	0
Clamped (C)	$u = 0, v = 0$	10^7	10^7	$u = 0, v = 0$	10^7	10^7
Simple-support 1 (S1)	$u = 0, \sigma_r = 0$	0	10^7	$u = 0, \sigma_\theta = 0$	10^7	0
Simple-support 2 (S2)	$u = 0, \tau_{r\theta} = 0$	10^7	0	$u = 0, \sigma_\theta = 0$	10^7	0
Elastic 1 (E1)	$u \neq 0, \tau_{r\theta} = 0$	10	0	$u \neq 0, \tau_{r\theta} = 0$	10	0
Elastic 2 (E2)	$v \neq 0, \sigma_r = 0$	0	10^2	$v \neq 0, \sigma_\theta = 0$	0	10^2
Elastic 3 (E3)	$u \neq 0, v \neq 0$	10^3	10^3	$u \neq 0, v \neq 0$	10^3	10^3

Table 4 Convergence of the first four frequency parameters for annular and sector plates with clamped boundary conditions for all the edges

		Present				Present*			
Shape	$M \times N$	1	2	3	4	1	2	3	4
Circular sector	7×7	2.8730	4.3624	4.4152	5.8891	3.2971	5.1626	5.2938	7.1833
	8×8	2.8793	4.3531	4.4001	5.8588	3.2143	5.0223	5.0687	6.8529
	9×9	2.8644	4.3567	4.4053	5.8059	3.1732	4.8899	4.9349	6.6820
	10×10	2.8645	4.3456	4.4116	5.7527	3.1296	4.8230	4.8342	6.5154
(Circular sector) [20]	11×11	2.8725	4.3428	4.3771	5.7839	2.9787	4.5141	4.5218	6.0085
	12×12	2.8725	4.3428	4.3771	5.7838	2.9660	4.4990	4.5153	5.9911
	13×13	2.8725	4.3428	4.3770	5.7838	2.9624	4.4930	4.4950	5.9829
	14×14	2.8725	4.3428	4.3770	5.7838	2.9531	4.4821	4.4903	5.9700
Annular sector	6×6	3.3657	4.4766	5.8209	5.9731	3.4874	4.8055	6.2316	6.4281
	7×7	3.3656	4.4766	5.8206	5.9726	3.4874	4.7204	6.1281	6.3018
	8×8	3.3656	4.4765	5.8171	5.9715	3.4874	4.6706	6.0666	6.2314
	9×9	3.3655	4.4765	5.8171	5.9715	3.4874	4.6378	6.0250	6.1860
	10×10	3.3654	4.4763	5.8155	5.9719	3.4874	4.7230	5.8342	6.5141
(Annular sector) [20]	10×10	3.3627	4.4742	5.8145	5.9651	3.4870	4.6523	6.0410	6.2141
	11×11	3.3627	4.4742	5.8145	5.9651	3.4870	4.6330	6.0380	6.1738
	12×12	3.3627	4.4742	5.8145	5.9651	3.4670	4.6224	6.0043	6.1708
	13×13	3.3627	4.4742	5.8144	5.9651	3.4670	4.6088	6.0021	6.1425
	14×14	3.3627	4.4741	5.8144	5.9651	3.4531	4.6011	5.9778	6.1404

Note: The results in bracket are from Ref. [20] with a much larger value of M and N. Present* means the results without considering the supplementary terms in the admissible functions.

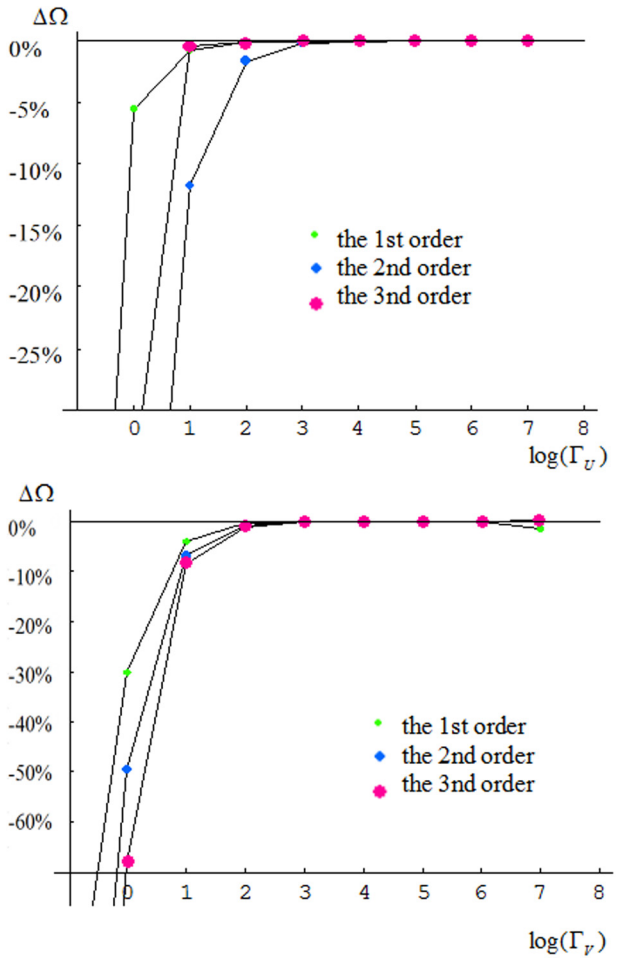

Fig. 2 Derivation of the frequency parameters versus the elastic boundary restraint parameters

Another important characteristic of the Fourier series is that the orthogonality with the trigonometric functions with respect to each other when integrated in the entire domain. To achieve the global stiffness matrix, the orthogonality property is very useful to reduce the effort in obtaining the matrix terms.

3 Numerical Results and Discussion

In this section, the convergence of the method is studied, and a systematic method to assign the values of nondimensional spring stiffness is discussed. A few numerical results are then compared to those by previous studies to demonstrate the excellent accuracy and reliability of the present method. A few computational examples on free in-plane vibration of circular sectorial and annular sector plates under various classical boundary conditions, elastic boundary conditions, demonstrate the extended applications of this method.

There are three kinds of materials in the examples, and their properties are listed in Table 2.

The shear elasticity $G_{r\theta}$ is defined according to $G_{r\theta} = E_\theta/2/(1-\mu_r\mu_\theta)$ as in Ref. [20]. For convenience, a nondimensional frequency parameter $\Omega = (2\omega R_1/\pi)\sqrt{(\bar{\rho}/(E_r(1-\mu_r\mu_\theta)))}$ is used in all the results, also the nondimensional stiffness of the attached springs is defined as $\tilde{K} = k_\gamma^\delta R_1(1-\mu_r\mu_\theta)/E_r$. A four-letter symbol is introduced to indicate the boundary conditions of annular and sector plates, starting with the first letter for the boundary condition of the edge at $r = R_0$ and going counterclockwise for subsequent letters (second letter for boundary condition at $\theta = 0$, etc.). The letters E^i ($i = 1, 2, 3$), S^j ($j = 1, 2$), C, and F denote type i elastic boundary, type j simply supported, clamped, and free boundary conditions, respectively. Nondimensional spring stiffness for these boundary conditions is given in Table 3. For example, the symbol E^1CFS^1 denotes an annular sector plate with E^1 elastic boundary condition at $r = R_0$, clamped at $\theta = 0$, free at $r = R_1$, and simply supported at $\theta = \phi$. For circular sectorial plate, the inner boundary reduces to a single point and is treated as free boundary, so a three-letter notation is used instead. For example, the symbol CFS^1 means that the plate is clamped at $\theta = 0$, free at $r = R_1$, and S^1 type simply supported at $\theta = \phi$.

For annular sector plate and circular sectorial plate, unless otherwise stated, the values of the following variables are: the outer radius $R_1 = 1$ m, the section angle $\phi = 90$ deg, and $h/R_1 = 0.001$.

Choosing appropriate number of terms in the truncated series is also important in the analysis. Table 4 shows the first four nondimensional frequency parameters of completely clamped circular sectorial and annular sector plates with different number of terms. The inner–outer radius ratio is $R_1/R_0 = 2$ for annular sector plate. From Table 4, the frequency converges fast and monotonically as the number of terms increases.

For circular sectorial plate, the convergence is also evident, though slightly slower. The value of R_0/R_1 should be small enough, but it cannot be zero because it will cause $\xi_{\min} = -\infty$. It was found out that a ratio of R_0/R_1 smaller than 1/20 yields satisfactory results. In this paper, the number of terms for the displacement functions is set as $M \times N = 10 \times 10$ in all the numerical examples. In previous studies, as the new logarithmic variable was not used, the number of terms was large in the truncated series to obtain accurate results (e.g., $M \times N = 15 \times 15$ is needed in the work of Wang et al. [20] to obtain satisfactory results).

Free vibration of clamped circular sectorial plate with $\phi = 90$ deg is investigated here. In Table 1, two ratios of $R_0/R_1 = 1/20$ and 1/40 are used. The spring stiffness values in both directions are assumed to be the same. The results show that the spring stiffness values should be sufficiently large to simulate the clamped boundary condition, for example, the nondimensional spring

Table 5 Comparison of frequency parameters for annular sector plate with various classical boundary conditions

B.C.	Mode number	1	2	3	4	5	6	7	8
CCCC	Present	3.3677	4.4791	5.8203	5.9742	6.7084	7.2168	7.7834	8.6131
	FEM^{AB} [20]	3.3692	4.4807	5.8240	5.9810	6.7152	7.2240	7.7894	8.626
$S^1S^1S^1S^1$	Present	1.5882	3.063	3.6308	4.4535	5.8097	6.0961	4.9339	6.4738
	FEM^{AN} [20]	1.5884	3.0641	3.6320	4.4572	4.9362	5.8163	6.1036	6.4793
$S^2S^2S^2S^2$	Present	1.3469	2.3639	2.8909	3.4244	3.5297	4.5766	4.7263	5.7089
	FEM^{AB} [20]	1.347	2.3646	2.8920	3.4255	3.5307	4.5787	4.7307	5.7165
CS^2CS^2	Present	3.3678	4.4783	5.8192	5.9732	6.7049	7.2154	7.7764	8.6112
	FEM^{AN} [20]	3.3680	4.4783	5.8191	5.9727	6.7048	7.2143	7.7746	8.6089
CS^1CS^1	Present	2.8909	3.3680	4.4783	5.7088	5.8191	5.9727	6.7048	7.2142
	FEM^{AN} [20]	2.8920	3.3690	4.4802	5.7164	5.8234	5.9802	6.7123	7.2234

Note: FEM^{AB} represents the ABAQUS software; FEM^{AN} represents the ANSYS software.

Table 6 Comparison of frequency parameters for annular sector plates with various boundary conditions

		CCCC			CFCF			FFFF			CCCF		
φ	Mode	Ref. [23]	Ref. [20]	Present	Ref. [20]	Ref. [19]	Present	Ref. [23]	Ref. [20]	Present	Ref. [23]	Ref. [20]	Present
$\pi/6$	1	5.4390	5.4393	5.4436	2.3213	2.3017	2.3283	3.2426	3.2426	3.2426	3.5475	3.5444	3.5382
	2	5.8784	5.8789	5.8892	4.1496	4.1843	4.1786	3.7879	3.7879	3.7880	4.5714	4.5641	4.5723
	3	6.8148	6.8151	6.8161	4.3005	4.2736	4.3020	3.8057	3.8057	3.8057	4.9758	5.0135	5.0201
	4	8.5272	8.5279	8.5292	5.5519	5.5842	5.5590	4.0817	4.0817	4.0817	6.8268	6.8501	6.8496
	5	8.8819	8.8826	8.8848	5.6386	5.5630	5.6419	5.1197	5.1197	5.1198	7.2006	7.2535	7.2587
	6	8.8889	8.8896	8.8875	6.2907	6.2801	6.2860	5.7187	5.7187	5.7190	7.6886	7.6896	7.6912
$\pi/2$	1	3.1705	3.1706	3.1711	2.5363	2.5249	2.5339	1.0433	1.0433	1.0433	2.6731	2.6788	2.6831
	2	4.2188	4.2189	4.2193	2.9806	2.9815	2.9852	1.7875	1.7875	1.7875	3.6268	3.6030	3.6011
	3	4.5757	4.5759	4.5756	3.9951	4.0516	3.9964	1.9884	1.9883	1.9883	4.3409	4.3005	4.3020
	4	4.5995	4.5995	4.6018	4.3390	4.3641	4.3373	2.9706	2.9706	2.9706	4.4260	4.4002	4.4187
	5	5.0436	5.0436	5.0437	4.3711	4.4014	4.3721	2.9782	2.9781	2.9783	4.6873	4.6596	4.6583
	6	5.4038	5.4038	5.4068	4.5207	4.5238	4.5228	3.1144	3.1143	3.1146	4.9093	4.9081	4.9090

Note: Here shear modulus $G = E_r \cdot (1 + \mu_r)/2$.

stiffness values of $\Gamma_U = \Gamma_V = 10^7$ are appropriate for $R_0/R_1 = 1/20$ and $\Gamma_U = \Gamma_V = 10^6$ for $R_0/R_1 = 1/40$ in the case of circular sectorial plate.

As to the boundary conditions, the classical boundary conditions can be imposed by assigning the attached massless springs with proper stiffness values. First, similar to the study of Wang et al. [20], we use two sets of springs in the normal and tangential directions to simulate the boundary conditions and vary the elastic spring stiffness values to study their effects on the plate's vibration frequency. The plate has an annular sector shape, and the boundary conditions are free at the two radial edges and restrained by one type of directional springs (either tangential or normal), with nondimensional stiffness values varying from 10^{-2} to 10^7 on the two circular edges. The variation in frequency parameter is defined as the difference in Ω for a certain Γ_λ ($\lambda =$ U and V) value to the case of $\Gamma_\lambda = 10^7$, i.e., $\Delta\Omega = \Omega_{\Gamma_\lambda} - \Omega_{\Gamma_\lambda = 10^7}$ is used in the calculation. The inner radius $R_0 = 0.5$ m, and the material is material A in Table 2. It is shown in Fig. 2 that for $\Gamma_\lambda (\lambda = U$ and $V)$ in the range of 10^{-2} to 10^7, $\Delta\Omega$ is negligible, thus aiding frequency convergence.

Table 3 summarizes the selected values of nondimensional spring stiffness for various classical boundary and elastic boundary conditions. It should be noted that the nonzero stiffness values of the elastic boundary conditions E^1, E^2, and E^3 are not unique and dependent on the types of springs.

Table 5 compares the results of an annular plate with various classical boundary conditions. The results from this study agree very well to those obtained by ABAQUS-v6.12 and ANSYS-v14.5 [20]. The results in Table 6 correspond to material C in Table 1. These results also agree very well with previous results reported by Singh and Muhammad [19], Wang et al. [20], and Shi et al. [23]. The previously mentioned analysis proves that the present method using the logarithmic radial variable is accurate and computationally efficient in handing in-plane vibration problems of annular sector plates or circular sectorial plates. Previous

Table 7 Normalized frequency parameters Ω for annular sector plates subject to classical boundary conditions and sector angle

			Sector angle		
B.C.	R_0/R_1	Mode no.	$\pi/3$	π	$5\pi/3$
CCCC	0.3	1	3.6099	2.1607	2.185
		2	5.2686	2.8594	3.5035
		3	5.7941	3.3794	2.8196
	0.8	1	7.41334 (7.4123)	7.1682 (7.1360)	7.1451 (7.1130)
		2	8.3091 (8.2781)	7.2727 (7.2407)	7.1833 (7.1513)
		3	9.5481 (9.5459)	7.4244 (7.4123)	7.2194 (7.2145)
$S^1S^1S^1S^1$	0.3	1	1.9743	1.0545	1.0398
		2	3.8205	1.3888	1.0927
		3	4.0126	1.9950	1.2950
	0.8	1	1.6481 (1.6413)	0.8461 (0.8441)	0.7701 (0.7688)
		2	3.0632 (3.0497)	1.2194 (1.2150)	0.9263 (0.9239)
		3	4.5357 (4.5162)	1.6481 (1.6413)	1.1402 (1.1364)
$S^2S^2S^2S^2$	0.3	1	2.3623	0.8476	0.5150
		2	4.2748	1.6298	1.0100
		3	4.3511	2.3624	1.4784
	0.8	1	2.1171 (2.1123)	0.7061 (0.7045)	0.4237 (0.4227)
		2	4.2254 (4.2159)	1.4119 (1.4088)	0.8473 (0.8454)
		3	6.3169 (6.3026)	2.1171 (2.1123)	1.2708 (1.2680)
FFFF	0.3	1	3.4695	2.3285	1.2074
		2	4.3455	2.8567	1.5800
		3	4.3789	3.4901	2.0651
	0.8	1	0.7985 (0.7973)	0.0829 (0.0828)	0.0279 (0.0278)
		2	1.9106 (1.9068)	0.2336 (0.2332)	0.0690 (0.0689)
		3	2.2122 (2.2097)	0.4720 (0.4711)	0.1519 (0.1516)

Note: The numbers in the parentheses are from Ref. [20].

Table 8 Normalized frequency parameters Ω for circular sectorial plates with various boundary conditions and sector angle

B.C.	R_0/R_1	Mode no.	Sector angle $\pi/3$	$2\pi/3$	π	$5\pi/3$
CCC	1/20	1	3.6276 (3.6106)	2.5097 (2.5067)	2.1819 (2.1557)	1.9134 (1.9100)
		2	5.1963 (5.1706)	3.6123 (3.6103)	2.8725 (2.8720)	2.2976 (2.2920)
		3	5.8099 (5.7842)	3.9971 (3.9838)	3.6171 (3.6081)	2.7299 (2.7247)
$S^2S^2S^2$	1/20	1	2.3618 (2.3568)	1.2545 (1.2514)	0.8605 (0.8586)	0.5287 (0.5278)
		2	4.3201 (4.3061)	2.3619 (2.3569)	1.6329 (1.6289)	1.0205 (1.0181)
		3	4.4538 (4.4439)	3.1367 (3.1371)	2.3697 (2.3569)	1.4782 (1.4793)
FFF	1/300	1	2.3583 (2.3659)	1.3811 (1.3889)	1.0509 (1.0780)	0.5356 (0.6073)
		2	2.9189 (2.8289)	2.3078 (2.3048)	1.7011 (1.7043)	1.1954 (1.2136)
		3	3.6896 (3.7296)	2.3829 (2.3910)	2.0267 (2.0424)	1.2983 (1.4421)
$E^1E^1E^1$ ($\Gamma_U = 10$)	1/20	1	2.1872	1.2206	0.8621	0.5002
		2	2.3325	2.2508	1.6074	0.9876
		3	3.1886	2.3530	1.6240	1.4577
$E^2E^2E^2$ ($\Gamma_V = 10^2$)	1/20	1	1.4689	1.0765	0.9124	0.9342
		2	2.3447	1.5030	1.4759	1.0854
		3	3.8137	2.3556	1.5166	1.3070
$E^3E^3E^3$ ($\Gamma_U = \Gamma_V = 10^3$)	1/20	1	3.6089	2.5065	2.1577	1.9186
		2	5.1695	3.6112	2.8723	2.2930
		3	5.7873	3.9825	3.6122	2.7253

Note: The numbers in the parentheses are from Ref. [20].

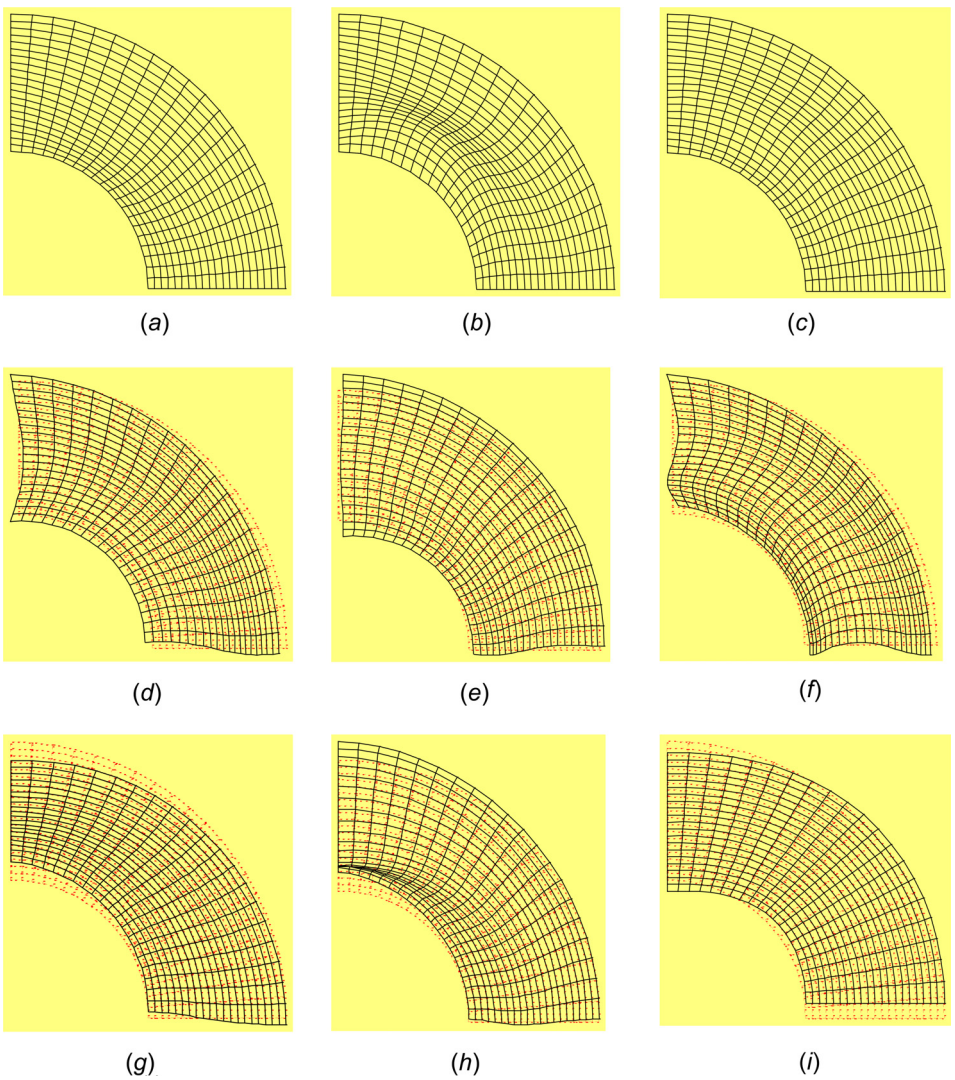

Fig. 3 The first three mode shapes of the annular sector plate with different boundary conditions: CCCC—(*a*) first, (*b*) second, and (*c*) third, FFFF—(*d*) first, (*e*) second, and (*f*) third, and $S^2S^2S^2S^2$—(*g*) first, (*h*) second, and (*i*) third

techniques usually are only applicable to certain combinations of boundary conditions and geometrical shapes of plate, but the method developed here can easily accommodate arbitrary boundary conditions and shapes by changing the corresponding input parameters.

More computational results are presented later to demonstrate the robustness and versatility of the method in this study. Table 7 shows the frequency parameters Ω of annular sector plates with various boundary conditions. Two values of R_0/R_1 (0.3 and 0.8) and three values of sector angle ($\pi/3$, π, and $5\pi/3$) are considered. Similarly, the frequency parameter Ω of circular sectorial plates with various boundary conditions is shown in Table 8. Four values of sector angle ($\pi/3$, $2\pi/3$, π, and $5\pi/3$) are considered. Here, the inner-to-outer radius ratio is taken as 1/300 for all but for the case of three-edge-clamped boundary, the ratio R_0/R_1 is taken as 1/20. It is shown that the sector angles ϕ and boundary conditions play dominant roles in the frequency parameters of circular sectorial plates. For the same values of inner-to-outer rations R_0/R_1 and same boundary conditions, the increase of the sector angle ϕ leads to decrease in the frequency.

After solving for the eigenvectors of the coupled eigenvalue problem in Eq. (30), the physical in-plane modal shapes can be easily calculated using Eq. (20). A few selected modal shapes of free in-plane vibration for annular sector plate are shown in Fig. 3.

4 Conclusions

In order to analyze the in-plane natural frequencies for the orthotropic sector plates with classical boundary conditions, a simplified solution procedure is developed based on the Ritz method with improved Fourier expansion. Introduction of the logarithmic radial variable significantly accelerates convergence and reduces computation cost. The developed method takes advantage of normal improved Fourier Ritz method without the new variable and exhibits many good characteristics such as good adaptability for any combination of boundary conditions and geometrical shapes and sizes, fast convergence, high reliability, and accuracy. The method is also applied to circular sectorial plate to demonstrate versatility and robustness.

According to the presented numerical results, the in-plane vibration characteristics of the plates mainly depend on the geometrical and material parameters and boundary conditions. It is found that for both annular sector and circular sectorial plates, the frequency parameters decrease monotonically as the sector angle increases if the other factors remain the same.

The method presented here is compared to the original theory that does not use the logarithmic radial variable, and the following four new characteristics are discussed:

(1) In the Ritz method with improved Fourier expansion for analyzing the in-plane vibration of sectorial plate, the basic theory for improved Ritz method and the solution procedure is significantly simplified.
(2) The admissible functions are simple in form with just trigonometric functions. The stiffness matrix and the mass matrix can be formulated in explicit forms, according to the several integration formulas in the Appendix. The stiffness matrix has many zero elements considering the orthogonality characteristics. Therefore, the method here is efficient in generating the global matrices.
(3) The range of nondimensional stiffness value for the boundary springs is discussed. Unless specially designated, a large value of 10^7 or 10^8 can be used for clamped boundary condition in numerical computation for satisfactory results (within 0.1% error).
(4) The number of terms in the truncated Fourier series for the displacement field is reduced to 10 for most cases and 11 for special cases where the inner radius is very small. Comparing with previous method that does not use the logarithmic radial variable (e.g., 15×15 terms in the work of Wang et al. [20]), the present method significantly reduces computation cost for the matrices dimensions in the eigenproblems, which is about 2/3 of that of Ref. [20].

Funding Data

- National Natural Science Foundation of China (Grant No. 11202146)

Nomenclature

a_{mn}, b_{mn}, c_{mn}, and d_{mn} = unknown coefficients
$A_{rr}, A_{\theta\theta}$, and $A_{r\theta}$ = the in-plane tensile stiffnesses (rigidities) $f_m(\xi)$
E_z ($z = r$ or θ) = Young's modulus in the z direction
$g_n(\theta)$ = admissible functions with variables ξ and θ
$G_{r\theta}$ = the shear elasticity
$G_{r\theta}$ = the shear Young's modulus
h = uniform thickness
$\tilde{K}$ = the nondimensional stiffness of the springs, where $\tilde{K} = k_\gamma^\delta R_1(1-\mu_r\mu_\theta)/E_r$
K^{uu}, K^{vv}, K^{uv} = the submatrices of the plate's global stiffness matrix
$\boldsymbol{K}^{uu}_{mnrs}, \boldsymbol{K}^{uv}_{mnrs}, \boldsymbol{K}^{vu}_{mnrs}, \boldsymbol{K}^{vv}_{mnrs}$ = the elements of the plate's global stiffness matrix
k_γ^δ = stands for the spring restraining stiffness
L = Lagrangian function
L_R = a constant defined as $\ln(R_1/R_0)$
M_{mnrs} = the elements of the plate's global mass matrix
$\boldsymbol{M}^{uu}, \boldsymbol{M}^{vv}$ = the submatrices of the plate's global mass matrix
$Q(r,\theta)$ = an arbitrary function
R_0 = inner radius
R_1 = outer radius
t = time
T = the kinetic energy of the sector plate
$T_{\max}$ = the maximum kinetic energy for the plate
u = displacements of the plate in the r direction
v = displacements of the plate in the θ direction
$V_{\max}$ = the maximum strain energy for the plate
V_{pl} = the strain energy of the sector plate
V_s = the potential energy
Γ_U = value of the nondimensional spring stiffness values in the r direction
Γ_V = value of the nondimensional spring stiffness values in the θ direction
μ_z ($z = r$ or θ) = Poisson's ratio in the z direction
ξ = variable defined as $\ln(r/R_0)$
ρ = the logarithmic radial variable
$\bar{\rho}$ = the plate's mass density
ϕ = sector angle
$\chi_m(r)$, $\zeta_n(\theta)$ = admissible functions with variables r and θ
$\Omega = (2\omega R_1/\pi)\sqrt{(\bar{\rho}/(E_r(1-\mu_r\mu_\theta)))}$ = nondimensional frequency parameter
ω = the frequency

Appendix

Useful integration

$$\int_0^L \cos(\lambda_m x)\cos(\lambda_n x)\mathrm{d}x = \begin{cases} 0 & m \neq n \\ \dfrac{L}{2} & m = n \neq 0 \\ L & m = n = 0 \end{cases} \tag{A1}$$

$$\int_0^L \sin(\lambda_m x)\sin(\lambda_n x)\mathrm{d}x = \begin{cases} 0 & m \neq n \\ \dfrac{L}{2} & m = n \neq 0 \\ 0 & m = n = 0 \end{cases} \tag{A2}$$

$$\int_0^L \sin(\lambda_m x)\cos(\lambda_n x)\mathrm{d}x = \begin{cases} \dfrac{\left(1-(-1)^{m+n}\right)Lm}{(m^2-n^2)\pi} & m \neq n \\ 0 & m = n \end{cases} \tag{A3}$$

$$\begin{aligned} &\int_0^L \cos(\lambda_m x)\cos(\lambda_n x)e^{ax}\mathrm{d}x \\ &= (-1)^{m+n}\frac{ae^{aL}}{2}\left(\frac{1}{a^2+(m+n)^2}+\frac{1}{a^2+(m-n)^2}\right) \\ &\int_0^L \sin(\lambda_m x)\sin(\lambda_n x)e^{ax}\mathrm{d}x \\ &= (-1)^{m+n}\frac{ae^{aL}}{2}\left(\frac{1}{a^2+(m-n)^2}-\frac{1}{a^2+(m+n)^2}\right) \quad (a=1,\,2) \\ &\int_0^L \sin(\lambda_m x)\cos(\lambda_n x)e^{ax}\mathrm{d}x \\ &= \left(1-(-1)^{m+n}\frac{ae^{aL}}{2}\right)\left(\frac{m-n}{a^2+(m-n)^2}+\frac{m+n}{a^2+(m+n)^2}\right) \end{aligned} \tag{A4}$$

where $\lambda_m = (m\pi/L)$ and $\lambda_n = (n\pi/L)$.

References

[1] Leissa, A. W., McGee, O. G., and Huang, C. S., 1993, "Vibrations of Circular Plates Having V-Notches or Sharp Radial Cracks," J. Sound Vib., **161**(2), pp. 227–239.

[2] Huang, C. S., Leissa, A. W., and McGee, O. G., 1993, "Exact Analytical Solutions for the Vibrations of Sectorial Plates With Simply Supported Radial Edges," ASME J. Appl. Mech., **60**(2), pp. 478–483.

[3] Jomehzadeh, E., and Saidi, A. R., 2009, "Analytical Solution for Free Vibration of Transversely Isotropic Sector Plates Using a Boundary Layer Function," Thin Walled Struct., **47**(1), pp. 82–88.

[4] Cheung, Y. K., and Kwok, W. L., 1975, "Dynamic Analysis of Circular and Sector Thick, Layered Plates," J. Sound Vib., **42**(2), pp. 147–158.

[5] Liew, K. M., Xiang, Y., and Kitipornchai, S., 1995, "Research on Thick Plate Vibration: A Literature Survey," J. Sound Vib., **180**(1), pp. 163–176.

[6] Onoe, M., 1956, "Contour Vibrations of Isotropic Circular Plates," J. Acoust. Soc. Am., **28**(6), pp. 1158–1162.

[7] Holland, R., 1966, "Numerical Studies of Elastic-Disk Contour Modes Lacking Axial Symmetry," J. Acoust. Soc. Am., **40**(5), pp. 1051–1057.

[8] Irie, T., Yamada, G., and Muramoto, Y., 1984, "Natural Frequencies of In-Plane Vibration of Annular Plates," J. Sound Vib., **97**(1), pp. 171–175.

[9] Leung, A. Y. T., Zhu, B., Zheng, J., and Yang, H., 2004, "Analytic Trapezoidal Fourier p-Element for Vibrating Plane Problems," J. Sound Vib., **271**(1–2), pp. 67–81.

[10] Lyon, R. H., 1986, "In-Plane Contribution to Structural Noise Transmission," Noise Control Eng. J., **26**(1), pp. 22–27.

[11] Farag, N., and Pan, J., 2003, "Modal Characteristics of In-Plane Vibration of Circular Plates Clamped at the Outer Edge," J. Acoust. Soc. Am., **113**(4), pp. 1935–1946.

[12] Chen, S. S., and Liu, T. M., 1975, "Extensional Vibration of Thin Plates of Various Shapes," J. Acoust. Soc. Am., **58**(4), pp. 828–831.

[13] Bashmal, S., Bhat, R., and Rakheja, S., 2009, "In-Plane Free Vibration of Circular Annular Disks," J. Sound Vib., **322**(1), pp. 216–226.

[14] Park, C. I., 2008, "Frequency Equation for the In-Plane Vibration of a Clamped Circular Plate," J. Sound Vib., **313**(1–2), pp. 325–333.

[15] Seok, J., and Tiersten, H., 2004, "Free Vibrations of Annular Sector Cantilever Plates—Part 2: In-Plane Motion," J. Sound Vib., **271**(3), pp. 773–787.

[16] Ravari, M. K., and Forouzan, M., 2011, "Frequency Equations for the In-Plane Vibration of Orthotropic Circular Annular Plate," Arch. Appl. Mech., **81**(9), pp. 1307–1322.

[17] Vladimir, N., Hadžić, N., Senjanović, I., and Xing, Y., 2014, "Potential Theory of In-Plane Vibrations of Rectangular and Circular Plates," Int. J. Eng. Modell., **27**(3–4), pp. 69–84.

[18] Kim, C.-B., Cho, H. S., and Beom, H. G., 2012, "Exact Solutions of In-Plane Natural Vibration of a Circular Plate With Outer Edge Restrained Elastically," J. Sound Vib., **331**(9), pp. 2173–2189.

[19] Singh, A., and Muhammad, T., 2004, "Free In-Plane Vibration of Isotropic Non-Rectangular Plates," J. Sound Vib., **273**(1), pp. 219–231.

[20] Wang, Q., Shi, D., Liang, Q., and Fazl e Ahad, 2016, "A Unified Solution for Free In-Plane Vibration of Orthotropic Circular, Annular and Sector Plates With General Boundary Conditions," Appl. Math. Modell., **40**(21–22), pp. 9228–9253.

[21] Li, W. L., 2000, "Free Vibrations of Beams With General Boundary Conditions," J. Sound Vib., **237**(4), pp. 709–725.

[22] Li, W. L., 2002, "Comparison of Fourier Sine and Cosine Series Expansions for Beams With Arbitrary Boundary Conditions," J. Sound Vib., **255**(1), pp. 185–194.

[23] Shi, X., Li, W., and Shi, D., 2014, "Free In-Plane Vibrations of Annular Sector Plates With Elastic Boundary Supports," Meetings on Acoustics Acoustical Society of America (ASA), Indianapolis, IN, Oct. 27–31.

[24] Zhang, K., Shi, D., Teng, X., Zhao, Y., and Liang, Q., 2015, "A Series Solution for the In-Plane Vibration of Sector Plates With Arbitrary Inclusion Angles and Boundary Conditions," J. Vibroeng., **17**(2), pp. 870–882.

[25] Du, J., Li, W. L., Jin, G., Yang, T., and Liu, Z., 2007, "An Analytical Method for the In-Plane Vibration Analysis of Rectangular Plates With Elastically Restrained Edges," J. Sound Vib., **306**(3–5), pp. 908–927.

[26] Jin, G., Ye, T., Chen, Y., Su, Z., and Yan, Y., 2013, "An Exact Solution for the Free Vibration Analysis of Laminated Composite Cylindrical Shells With General Elastic Boundary Conditions," Compos. Struct., **106**, pp. 114–127.

[27] Chen, Y., Jin, G., and Liu, Z., 2014, "Flexural and In-Plane Vibration Analysis of Elastically Restrained Thin Rectangular Plate With Cutout Using Chebyshev–Lagrangian Method," Int. J. Mech. Sci., **89**, pp. 264–278.

[28] Wang, Q., Shi, D., Liang, Q., and Shi, X., 2016, "A Unified Solution for Vibration Analysis of Functionally Graded Circular, Annular and Sector Plates With General Boundary Conditions," Composites, Part B, **88**, pp. 264–294.

[29] Wang, Q., Shi, D., and Shi, X., 2016, "A Modified Solution for the Free Vibration Analysis of Moderately Thick Orthotropic Rectangular Plates With General Boundary Conditions, Internal Line Supports and Resting on Elastic Foundation," Meccanica, **51**(8), pp. 1985–2017.

[30] Yao, W., Zhong, W., and Lim, C. W., 2009, *Symplectic Elasticity*, World Scientific, Singapore.

[31] Kim, K., and Yoo, C. H., 2010, "Analytical Solution to Flexural Responses of Annular Sector Thin-Plates," Thin-Walled Struct., **48**(12), pp. 879–887.

[32] Dozio, L., 2010, "Free In-Plane Vibration Analysis of Rectangular Plates With Arbitrary Elastic Boundaries," Mech. Res. Commun., **37**(7), pp. 627–635.

[33] Gorman, D. J., 2006, "Exact Solutions for the Free In-Plane Vibration of Rectangular Plates With Two Opposite Edges Simply Supported," J. Sound Vib., **294**(1–2), pp. 131–161.

[34] Budiansky, B., and Hu, P. C., 1946, "The Lagrangian Multiplier Method of Finding Upper and Lower Limits to Critical Stresses of Clamped Plates," NASA Langley Research Center, Hampton, VA, Technical Report No. 848.

[35] Ilanko, S., Monterrubio, L., and Mochida, Y., 2014, *The Rayleigh-Ritz Method for Structural Analysis*, Wiley, Hoboken, NJ.

[36] Monterrubio, L. E., and Ilanko, S., 2015, "Proof of Convergence for a Set of Admissible Functions for the Rayleigh–Ritz Analysis of Beams and Plates and Shells of Rectangular Planform," Comput. Struct., **147**, pp. 236–243.